Thesis
Study of two-track separation in a jet chamber

Tokyo University of Agriculture and Technology
Kuroiwa Hirotoshi

Abstract

Two-track separation capability of a small jet-cell type drift chamber has been studied as a part of the R&D program on the JLC-CDC(Japan Linear Collider - Central Drift Chamber). The test chamber constructed specially for this study consists of three jet cells, each having five sense wires and a maximum drift length of 50mm. The chamber is operated with a CO_2-isoC_4H_{10}(90:10) gas mixture.

The performance of the test chamber has been studied by using the electron and photon beams at the KEK-Tanashi 1.3-GeV electron synchrotron. For isolated single tracks, an average spatial resolution better than 100μm is obtained over the full drift space. Two tracks with a track distance of greater than 5mm are identified without ambiguity.

The thesis describes the experimental procedure, the analysis, and the results in detail.

Contents

1 Introduction **3**

2 Experiment **5**
2.1 Test chamber 5
2.1.1 Cell structure 5
2.1.2 H.V. and electric field 5
2.2 Experimental setup 9
2.2.1 Electronics and DAQ system 9
2.2.2 Gas system 10
2.2.3 Adjustment of the chamber position 11
2.3 Experiment 14
2.3.1 Electron and photon beams 14
2.3.2 Single track runs 14
2.3.3 Two-track runs with e^+e^- pairs 14

3 Analysis, Results, and Discussions **15**
3.1 Analysis procedure 15
3.1.1 Pulse cluster finding and time measurement 15
3.1.2 T_0 determination 15
3.1.3 x-t relation 17
3.2 Gas gain saturation problem 18
3.3 Pulse shape analysis 24
3.4 Analysis of the single track data 24
3.4.1 Track fitting 24
3.4.2 Wire efficiency 27
3.4.3 Spatial resolution 27
3.5 Two-track separation 37

3.5.1 Two-track separation probability 37
3.5.2 Effect of the gas gain saturation problem 37

4 Conclusion **43**

5 Acknowledgment **45**

Chapter 1

Introduction

A cylindrical drift chamber has been a primary choice for the central tracker at most collider experiments because of its high cost performance in terms of spatial resolution and geometrical acceptance without introducing massive materials to spoil performance of the surrounding detectors such as calorimeters. This tradition will continue with experiments at a future linear e^+e^- collider such as JLC, provided that we can achieve high enough momentum resolution for ever higher energy particles produced in ever jettier environment.

The proudction of hadronic jets is a direct consequence of color confinment which is characterized by a hadronization scale of order a few 100 MeV: colored partons such as quarks and gluons are produced in e^+e^- annihilation as a color singlet system. In the beginning these colored partons move apart freely with energies proportional to the beam energy. When they are separated by a spatial distance greater than the inverse of the hadronization scale, they can no longer exist as free particles. They are bound with a color string and this color string breaks up to form multiple hadrons. Since the produced hadrons stem from the moving string in the initial parton direction, their longitudinal momenta roughly sum up to its parent parton momentum which is proportinal to the beam energy. On the other hand, their transverse momenta are characterized by the hadronization scale which is independent of the beam energy. The produced hadrons are thus collimated into a narrow cone: the higher the energy the narrower the cone. This phonomenon is called hadronic jet production.

The central tracker should be able to identify each charged track in a

jet and to measure its momentum to a high precision. This is particularly important when one wants to separate, say, W bosons from Z bosons by means of jet invariant mass measurements: it requires both high momentum resolution and efficient matching to calorimeter clusters for individual tracks in the jet. The number of charged tracks in a W boson decay is in excess of 25 on average resulting in a very high track density. This is why two-track separation, which is a measure of capability to identify individual tracks under a high track density environment and is defined to be the minimum distance of two tracks separable as two tracks, becomes so important at high energies. Monte Carlo studies show that spatial resolution better than 100 μm and two-track separation better than 2mm are required for the central tracker of the JLC detector.

We have been carrying out a consistent R&D program for a possible candidate of the JLC central tracker, which is a large cylindrical drift chamber with a small jet cells. The study presented in this thesis is a part of this R&D program and focuses on the basic chamber performance including spatial resulution, efficiency, and two-track separation as determined by the cell design, gas mixture choice, etc. We have built a test chamber with a candidate cell structure filled with a possible gas mixture CO_2-isoC_4H_{10}(90:10) for this purpose and made a beam test with special emphasis put on two-track separation study. The beam test was carried out at the $\gamma 2$ beam line of the 1.3-GeV KEK-Tanashi Electron Synchrotron (ES), using an extracted electron beam for studying single track performance, or using a bremsstrahlung photon beam converted to e^+e^- pairs for studying two-track separation capability.

This thesis is organized as follows. Chapter 2 begins with a description of the test chamber itself, which is followd by a sketch of our experimental setup. A short summary of experimental procedure and data taking is given at the end of this chapter. Chapter 3 comprises the main body of the thesis and contains a detailed account of the data analysis and results on basic chamber performance derived from the single track and two-track data, separately. Discussions on the results are also given in this chapter. Finally, Chapter 4 summarizes the results and concludes the thesis.

Chapter 2

Experiment

2.1 Test chamber

2.1.1 Cell structure

In order to test the overall performance including two-track separation capability, we constructed a test chamber with small jet cells, which is called hereafter a *baby* chamber of the proposed JLC-CDC. Figure 2.1 shows a picture of the test chamber, while figure 2.2 shows its cell structure. The cross-sectional size of the test chamber is 26cm $\times$ 27cm and the wire length is 40cm. This chamber has three identical jet cells (cell1 to cell3), each being 7cm $\times$ 10cm in size and having five sense wires (s1 to s5) and a maximum drift length of 5cm. The sense wire spacing is 1cm. These sense wires are made of Au-plated W and have a diameter of 30μm. Other wires are made of Au-plated Al and are 125μm thick.

2.1.2 H.V. and electric field

Figure 2.3 shows the high voltage applied on each wire and equipotential lines in the cell. Plotted in figure 2.4 are, on the other hand, the drift lines and iso-chrons calculated with the drift chamber simulation program GARFIELD. The high voltage on the sense wire is 2.8kV and the electric field in the drift space is 1.0kV/cm. The H.V. on each wire was decided based on the following criteria:

- the electric field in the drift region has to be as uniform as possible,

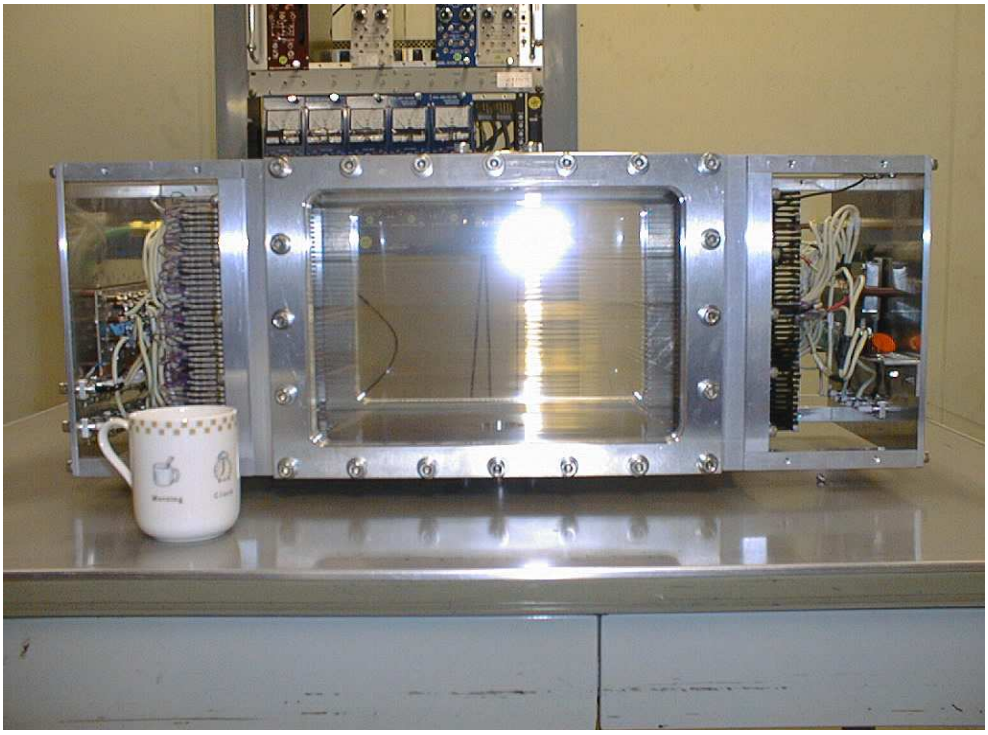

Figure 2.1: the test chamber

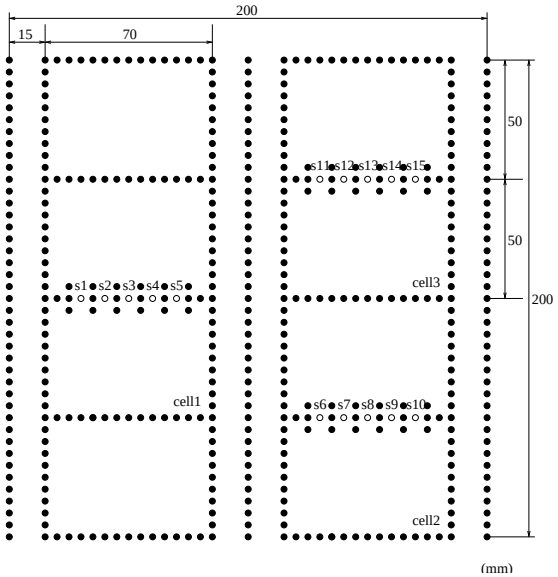

Figure 2.2: cell structure of the test chamber

- corresponding drift velocity and diffusion for track electrons have to be small enough for required spatial resolution and two-track separation,
- the electrostatic force on wires has to be small enough to assure mechanical cell stability,
- the sense wire gas gain has to be of about 10^5, while the surface fields on other wires should not exceed 20kV/cm.

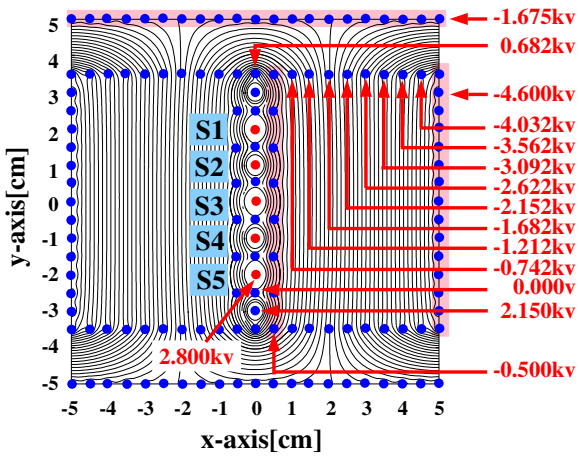

Figure 2.3: H.V. on each wire and the equipotential lines in the cell

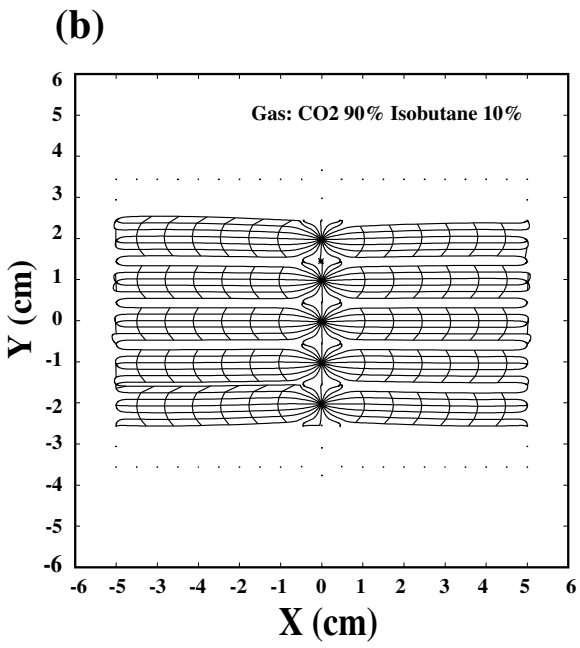

Figure 2.4: drift lines and iso-chrons in the cell

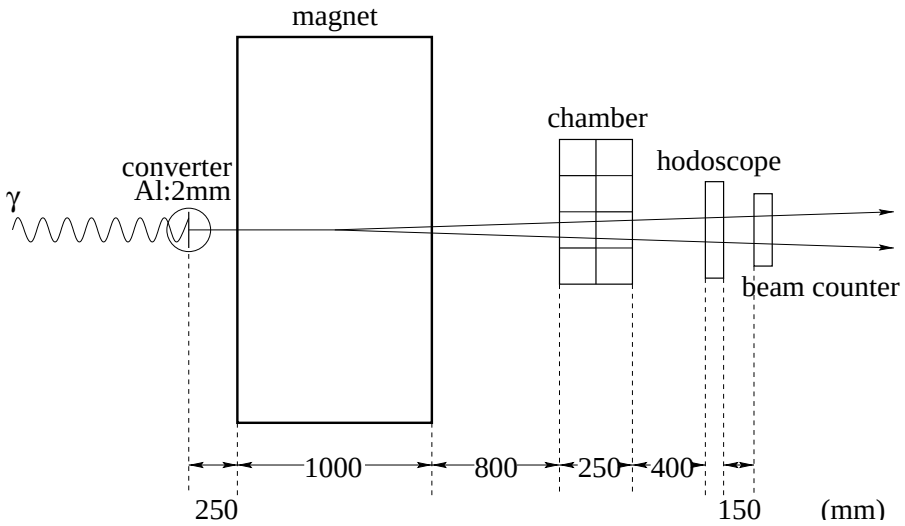

Figure 2.5: set up for the two-track separation experiment (side view)

2.2 Experimental setup

The experiment was carried out at the $\gamma 2$ beam line of the KEK-Tanashi 1.3-GeV Electron Synchrotron. The experimental setup for the two-track separation study is shown in figure 2.5.

In this experiment, we used a hodoscope and a beam counter as triggering devices. The hodoscope has eight channels in both horizontal and vertical directions and each channel consists of a 2mm wide scintillation counter.

2.2.1 Electronics and DAQ system

Current preamplifiers are mounted on the endplate of the test chamber. The signals from the preamplifiers go into flashADCs after passing through post amplifiers. The flashADCs have 8bits and a 500MHz sampling frequency over a 1.6μsec time window. The time bin width of one channel is 2nsec. We used this fast flashADC because we can,

- analyze the pulse shape,

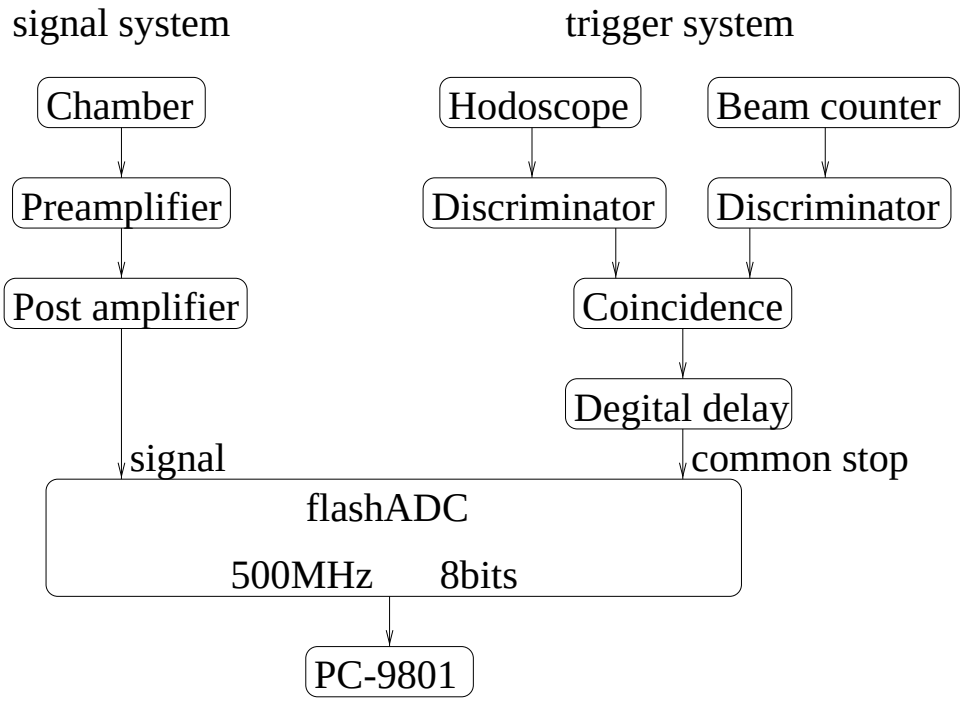

Figure 2.6: block diagram

- separate close tracks,
- make a clear distinction between the signal and the noise.

Figure 2.6 shows a block diagram of our data aquisition system.

2.2.2 Gas system

In this experiment, we used a CO_2-isoC_4H_{10}(90:10) mixture as our chamber gas. The chamber was continuously flushed through with a fresh gas mixture throughout the experiment. The flow rate of each component gas was controlled by a mass flow controller and determined the mixing ratio. These component gases were mixed while passing through an O_2 filter and flowed into the chamber. The flow rates of CO_2 and isoC_4H_{10} were kept at 180cc/min and 20cc/min, respectively.

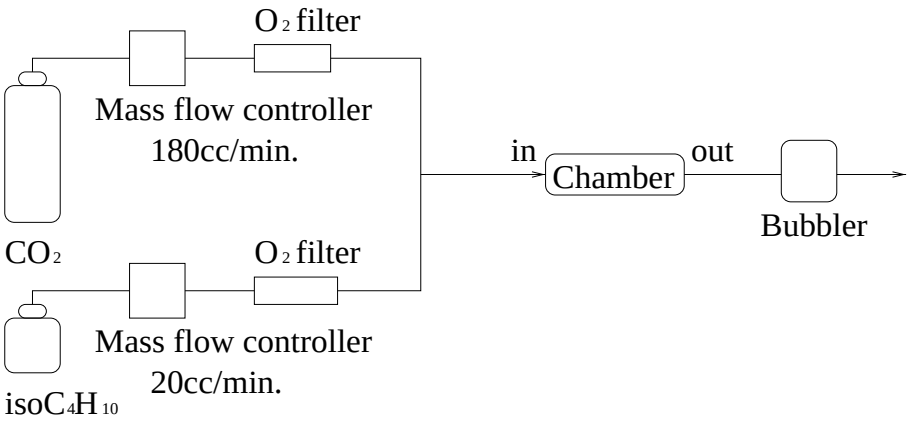

Figure 2.7: gas system

Figure 2.7 shows a block diagram of the gas system.

2.2.3 Adjustment of the chamber position

In this experiment, in order to change the incident position of the beam we adjusted the chamber position by means of a movable support table. This adjustable support system is shown in figure 2.8. The chamber was mounted on a stage movable in the vertical direction so as to adjust the incident position of the beam or the drift distance in other words.

This stage is also rotatable in the θ and ϕ directions as depicted in figure 2.9. If the stage rotates in the θ direction, an angle is produced between the beam and the wires. A rotation in the ϕ direction produces an angle between the beam and the equipotential line. We measured the performance for $\theta =$ 10, 20, and 30 digrees and for $\phi = 10$, 20, and 30 digrees.

In all cases, the beam was injected into the lower half of the cell1.

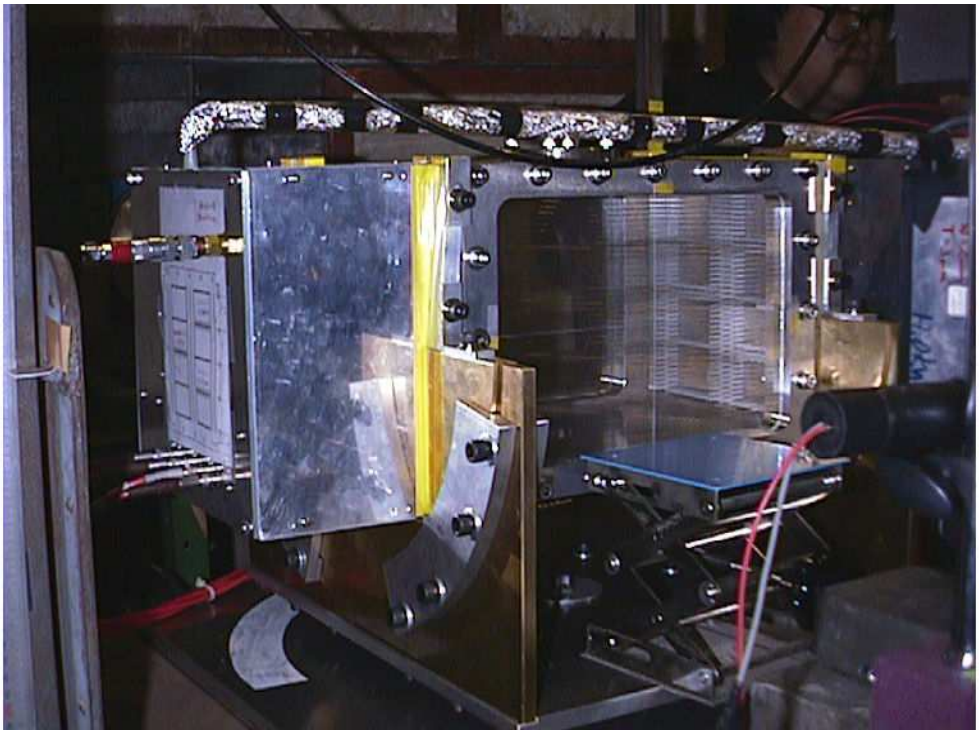

Figure 2.8: test chamber on the movable stage

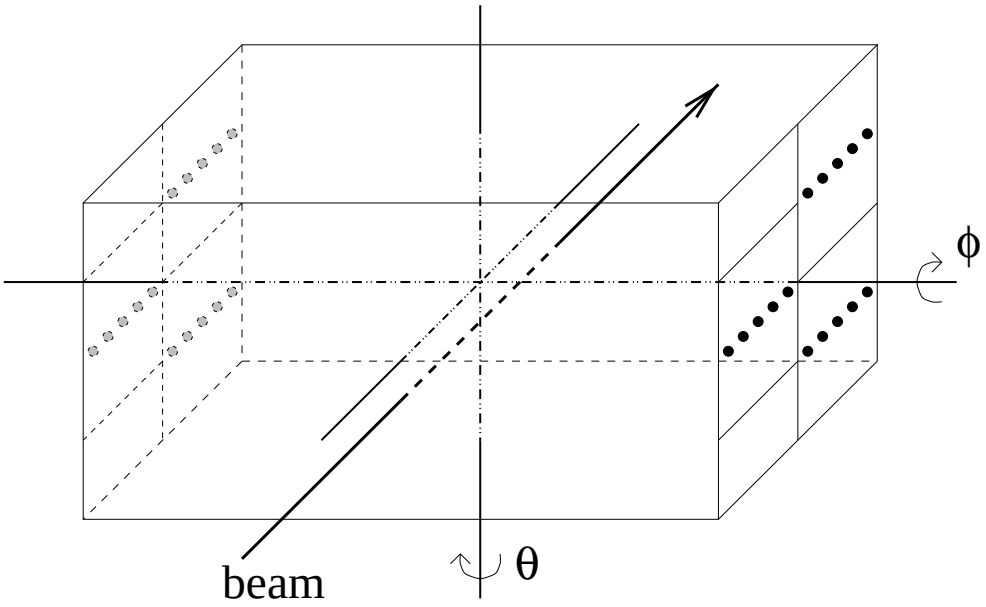

Figure 2.9: definitions of θ and ϕ

2.3 Experiment

2.3.1 Electron and photon beams

In the case of single track data taking, the electron beam extracted from the electron synchrotron (ES) was used. In the case of two-track data taking, we used a bremsstrahlung photon beam produced at a Pt radiator. This γ-ray beam was converted to electron-positron pairs by an Al plate converter (thickness:2mm). These electron-positron pairs were separated vertically by a magnetic field controlled to generate two tracks with various track-to-track distance in the drift chamber.

2.3.2 Single track runs

In single track runs, we took the following data. First, we measured eleven injection positions of the beam, corresponding to drift lengths set at every five millimeters from 0cm to 5cm. In this case, the beam was perpendicular to the chamber. In the following, these data will be used to get x-t relation and then to study basic performance of this chamber. In addition, we took the data for inclined tracks in order to study angle dependence. In the case of θ rotations, the drift length was kept at 2.5cm. In the case of ϕ rotations, the drift lengths for sense wire #3 were 0.5cm, 2.5cm, and 4.5cm.

2.3.3 Two-track runs with e^+e^- pairs

In two-track runs, we took data for drift lengths of 1.0cm, 2.5cm, and 4.0cm. The beam was nearly perpendicular to the drift region.

Chapter 3

Analysis, Results, and Discussions

3.1 Analysis procedure

3.1.1 Pulse cluster finding and time measurement

Typical sense wire signal shapes for a single track are shown in figure 3.1 as recorded by flashADCs. The horizontal axis is drift time (nsec) and the vertical axis is pulse height (flashADC counts). The distance between sense wires and the cell boundary is 5cm. The drift velocity in the CO_2-isoC_4H_{10}(90:10) gas mixture was measured to be 6mm/μsec at 1kV/cm. Therefore, the maximum drift time is 8400nsec. The event in the figure thus corresponds to a track passing perpendicularly through the center of the drift region.

Any pulse which continues longer than 80nsec above the threshold (pedestal+five counts) was regarded as a signal pulse. The arrival time of the signal pulse was determined by its leading edge at which the pulse height exceeded the threshold.

3.1.2 T_0 determination

The so called T_0 (the signal arrival time for the zero drift length) was determined from the shorter-drift-length edge of the arrival time distribution for each sense wire where the electron beam was injected just on the sense

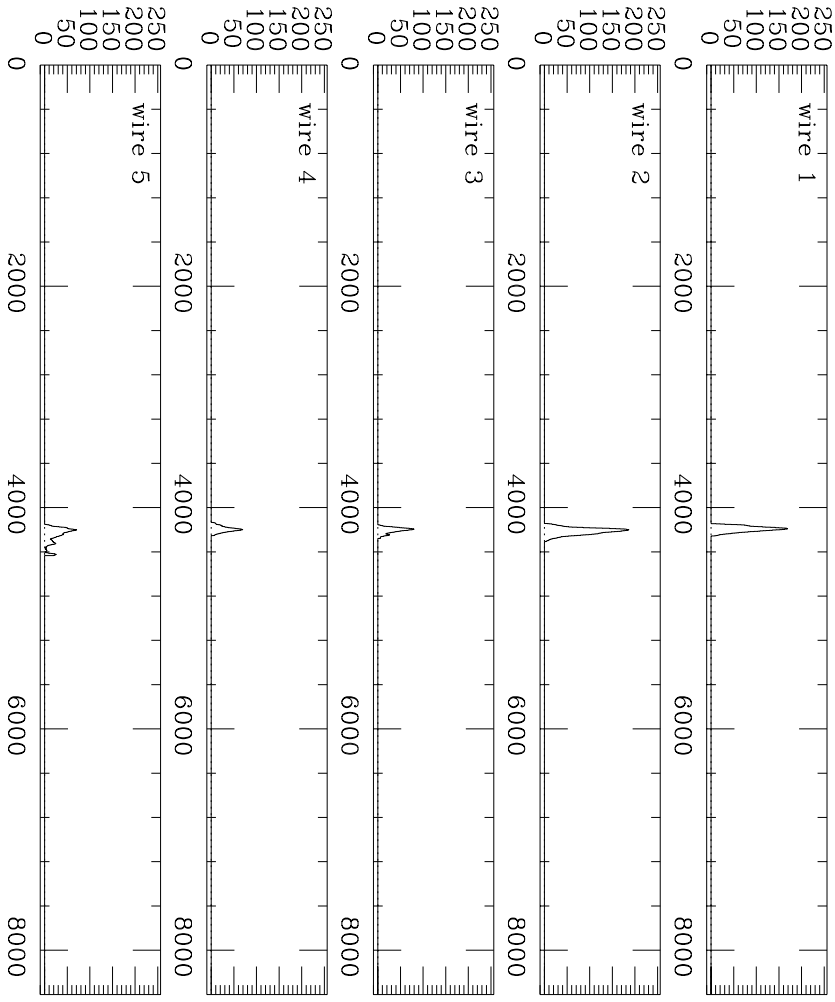

Figure 3.1: typical pulse shapes for a single track

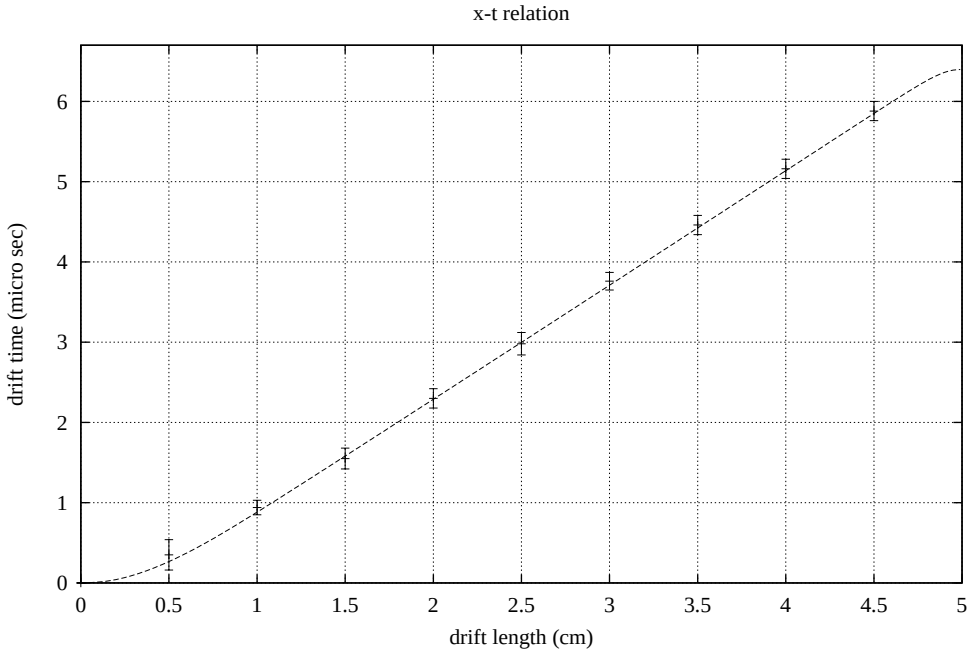

Figure 3.2: comparison of the data (points with error bars) with the x-t relation calculated with GARFIELD (the dotted line) for the central sense wire

wire. The drift time can then be defined as the arrival time measured from T_0.

3.1.3 x-t relation

In order to convert the drift time to the drift length, we used the x-t relation calculated with GARFIELD for each wire. The validity of the calculated x-t relation was experimentally confirmed by comparing the drift velocity given by GARFIELD with the independent drift velocity measurements. The x-t relation is compared with the beam data in figure 3.2 for the central sense wire (s3), showing a good agreement.

3.2 Gas gain saturation problem

The number of pulses per event for each sense wire is shown in figure 3.3 for single track data. More than 50% of the times, however, we have more than two pulses, which is a potential problem for two-track separation. Therefore, we consider this phenomenon first.

Figures 3.4 and 3.5 show peak heights plotted against drift times of the first and second pulses, respectively, for the central sense wire (s3), using the same single track data. From these figures, we can see, in each event, that a big pulse arrived first at the sense wire which was followed by a small pulse. We call, hereafter, the first arriving pulse *pulse1* and the second pulse *pulse2*, and so on. The time difference between *pulse1* and *pulse2* was 200 to 400nsec as seen from figure 3.6. This time difference corresponds to 1.2 to 2.4mm in terms of drift distance, which is comparable to our required two-track separation capability. In what follows, we investigate possible causes of this phenomenon.

The first question to ask is whether our electronics system has a problem or not. The time difference between *pulse1* and *pulse2* is histogrammed in figure 3.6, where the horizontal axis is in units of nsec. On the other hand, the peak pulse height of *pulse1* is plotted against the peak pulse height of *pulse2* in figure 3.7. If the electronics system caused two pulses, the time difference between *pulse1* and *pulse2* should be constant and there should be a correlation between the peak pulse height of *pulse1* and *pulse2*. But, the time difference was not constant and the correlation was not seen between the peak pulse height of *pulse1* and *pulse2*. Therefore, we considered that the cause of two pulses was not the electronics problem.

The next question is whether this phenomenon is caused by some electronic cross talk between the wire and the wire or not. The number of pulses for $\phi = 20°$ is shown in figure 3.8 for the central sense wire (s3) (see figure 2.9 for the definition of the angle ϕ). The number of events with more than two pulses is more than that for the perpendicular beam data in figure 3.3. The peak pulse height of *pulse1* is plotted against the time difference between *pulse1* and *pulse2* in figure 3.9 $\phi = 20°$. If the second pulse was coming from any cross talk, the time difference for $\phi = 20°$ should be different from that of figure 3.6. There is, however, no such significant difference. We thus conclude that it is not any cross talk.

This leaves the gas gain saturation as the remaining possibility. In short,

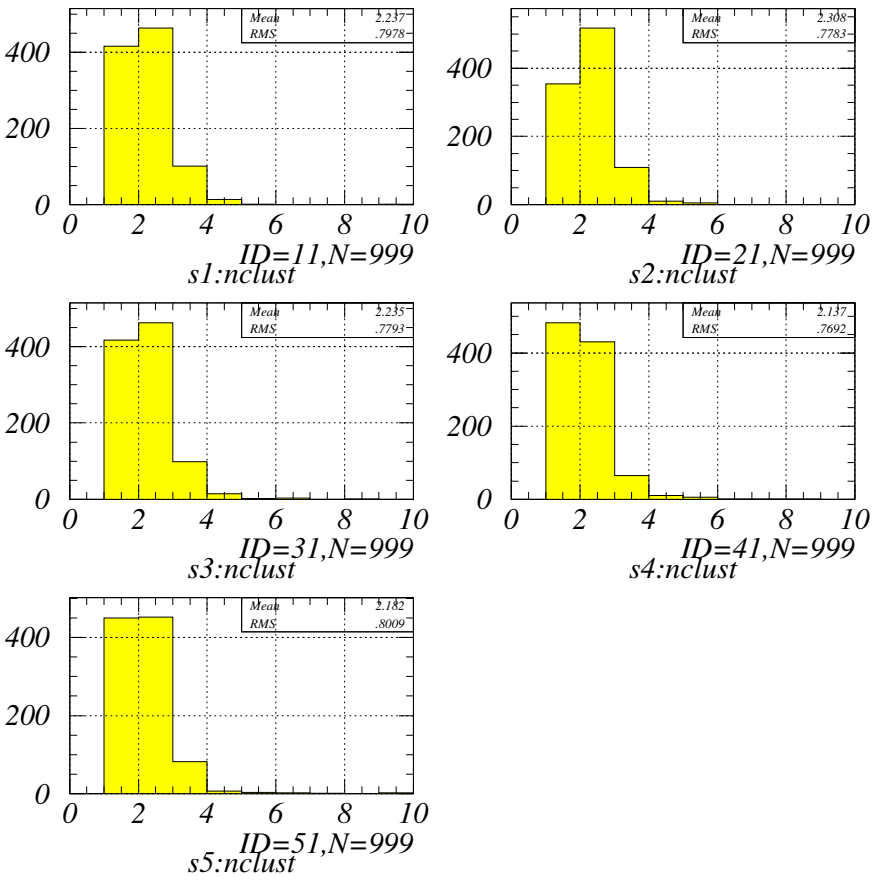

Figure 3.3: the number of pulses per event for each sense wire for single track data

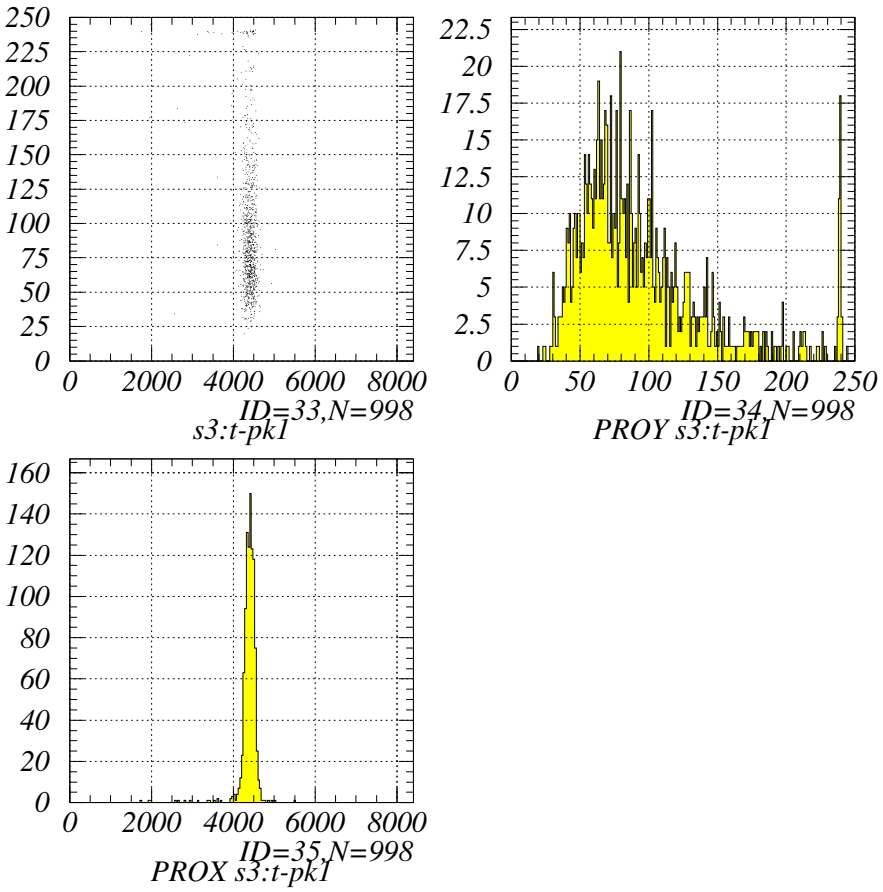

Figure 3.4: peak pulse height of *pulse1* plotted against its drift time for the central sense wire (s3)

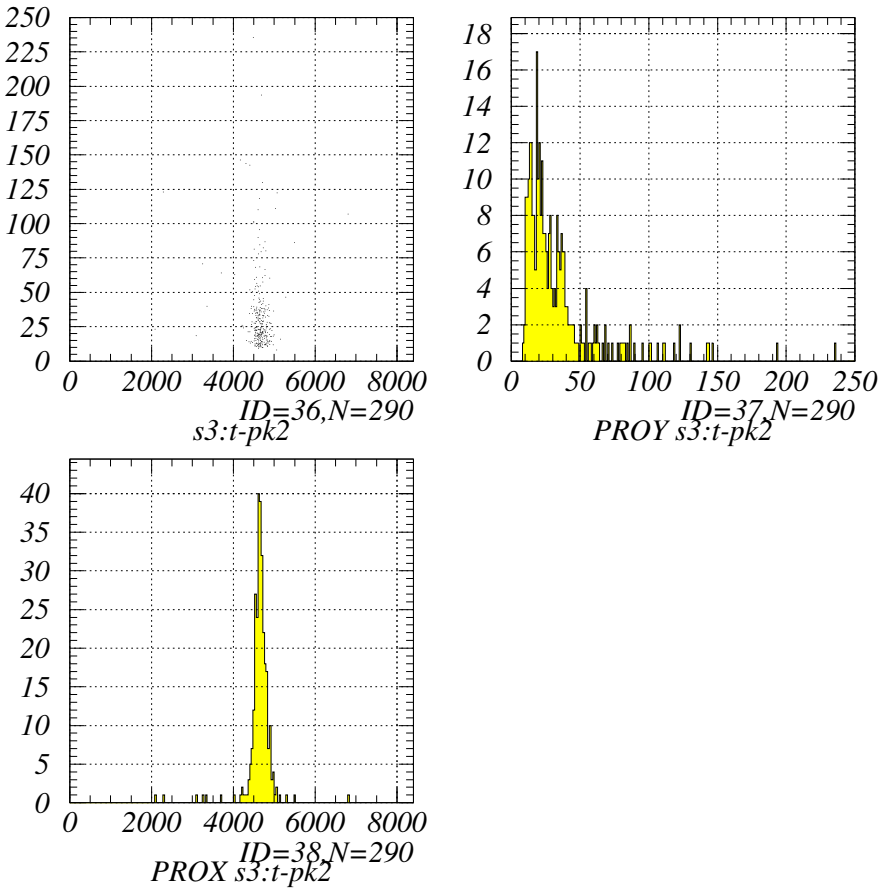

Figure 3.5: similar plots to figure 3.4 but for *pulse2*

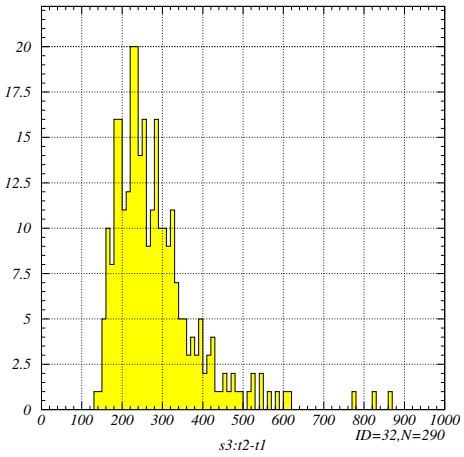

Figure 3.6: time difference between *pulse1* and *pulse2* for the central sense wire (s3)

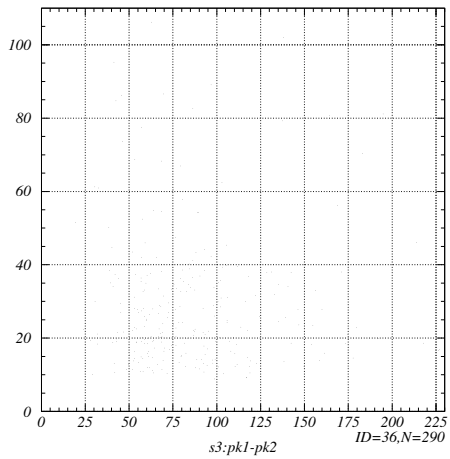

Figure 3.7: peak pulse height of *pulse1* plotted against the peak pulse height of *pulse2* for the central sense wire (s3)

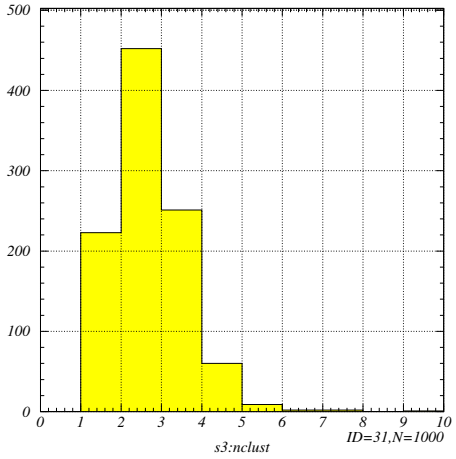

Figure 3.8: the number of pulses per event for $\phi = 20°$ for the central sense wire (s3)

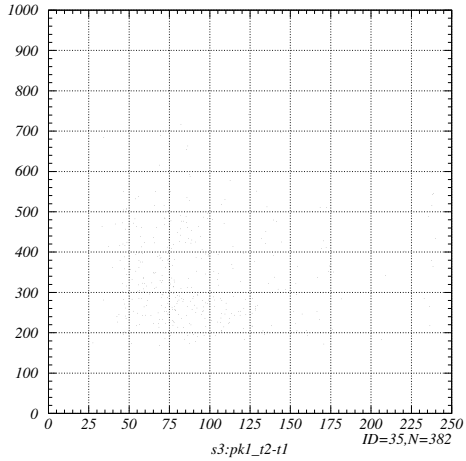

Figure 3.9: peak pulse height of *pulse1* plotted against the time difference between *pulse1* and *pulse2* for $\phi = 20°$ (s3)

the phenomenon can be explained as follows. The diffusion is very small in the CO_2-isoC_4H_{10}(90:10) mixture. The electrons that arrive first at a sense wire cause an avalanche in the strong electric field around the wire. This is *pulse1*. The avalanche is concentrated on a point near the wire because of very small diffusion and produces a cluster of space charge. This space charge causes a dead time. Only after this dead time has been recovered, any late arriving track electrons can form *pulse2*.

3.3 Pulse shape analysis

We analyzed about the pulse shape and compared this pulse shape with the pulse shape calculated with GARFIELD. The pulse shape of this experiment is shown in figure 3.10. This figure shows the pulse shape averaged all the *pulse1* measured in the same condition (drift distance of 2.5cm). The pulse shape calculated with GARFIELD is shown in figure 3.11. The condition of figure 3.10 and figure 3.11 is almost the same. But figure 3.11 shows the pulse shape of only one event (not average). From figure 3.10, the pulse width in this experiment was 80nsec. But the pulse width in figure 3.11 is more than 100nsec. From these figures, we considered that the space charge caused a dead time and the cause of two pulses was this dead time by the gas gain saturation.

3.4 Analysis of the single track data

3.4.1 Track fitting

Before track fitting, we tried to remove *pulse2* in order to avoid fake tracks, by requiring peak height be greater than 20 flashADC counts (see figure 3.4). In this analysis, we use residual distributions to calculate spatial resolutions. A residual is the distance between an actual hit on the wire in question and the expected hit from the track obtained by fitting the hits on the other four wires (see figure 3.12). The spatial resolution is then calculated by subtracting track error off the residual distribution. It is important to eliminate the wire in question from track fitting, since, otherwise, it pulls the reference track towards the actual hit, therely making apparent resolution better than reality.

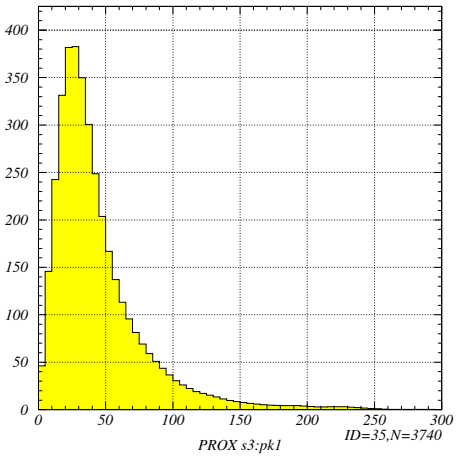

Figure 3.10: the averaged pulse shape of this experiment (drift distance of 2.5cm)

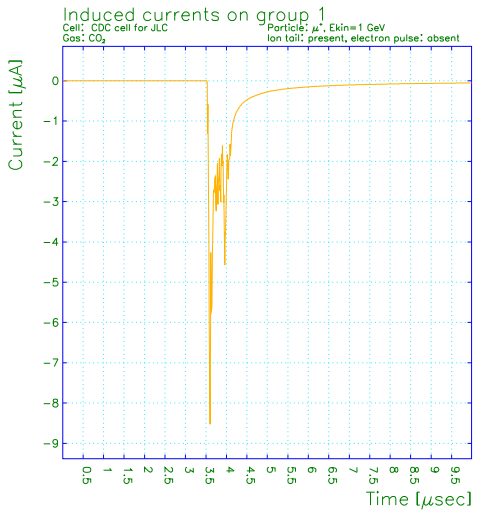

Figure 3.11: the pulse shape of one event calculated with GARFIELD (drift distance of 2.5cm)

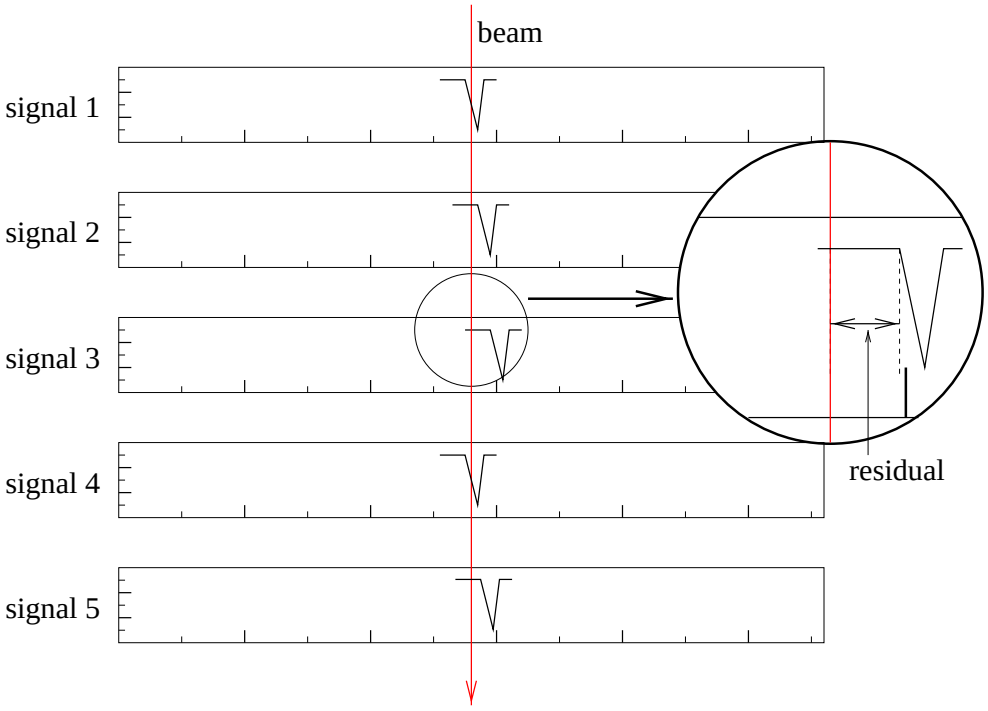

Figure 3.12: definition of the residual

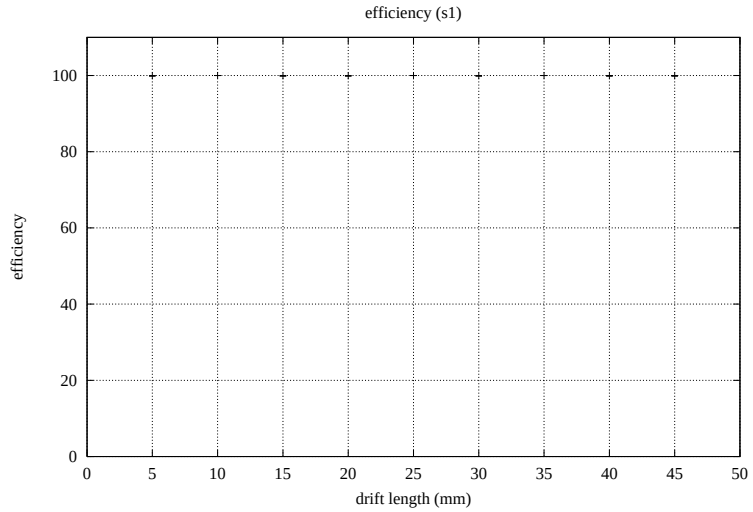

Figure 3.13: efficiency as a function of the drift distance for s1

3.4.2 Wire efficiency

The efficiencies for individual sense wires are shown in figures 3.13 to 3.17 as functions of the drift length, using a 5σ window. The figures demonstrate that the efficiency of this test chamber is essentially 100% everywhere.

3.4.3 Spatial resolution

The residual distributions for individual sense wires are shown in figure 3.18. The spatial resolutions were calculated by taking track error off and plotted in figures 3.19 to 3.23 as functions of the drift length. The overall spatial resolution of this test chamber is less than 100μm.

The residual distributions for different θ angles are shown in figure 3.24, while the residual distributions for different ϕ angles are shown in figure 3.25. The spatial resolution is less than 100μm regardless of the incident angles.

Figure 3.26 shows the peak pulse height as a function of the drift time for the central sense wire (s3). The horizontal axis is the drift time (nsec) and the vertical axis is the peak pulse height (flashADC counts). The peak pulse

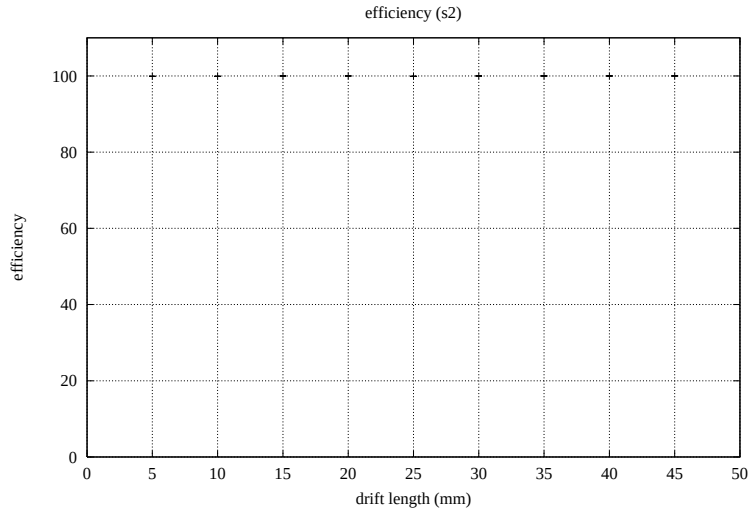

Figure 3.14: efficiency as a function of the drift distance for s2

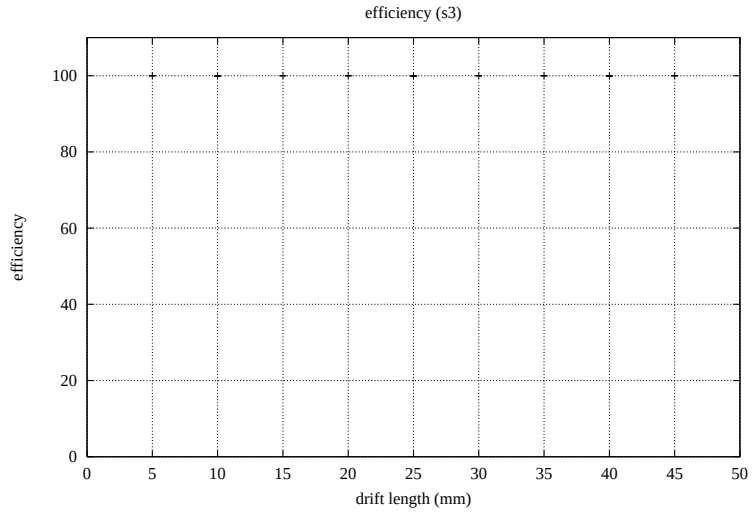

Figure 3.15: efficiency as a function of the drift distance for s3

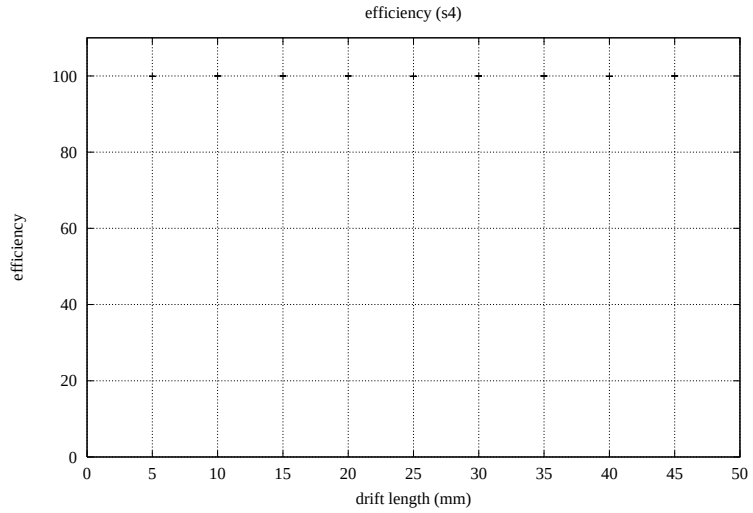

Figure 3.16: efficiency as a function of the drift distance for s4

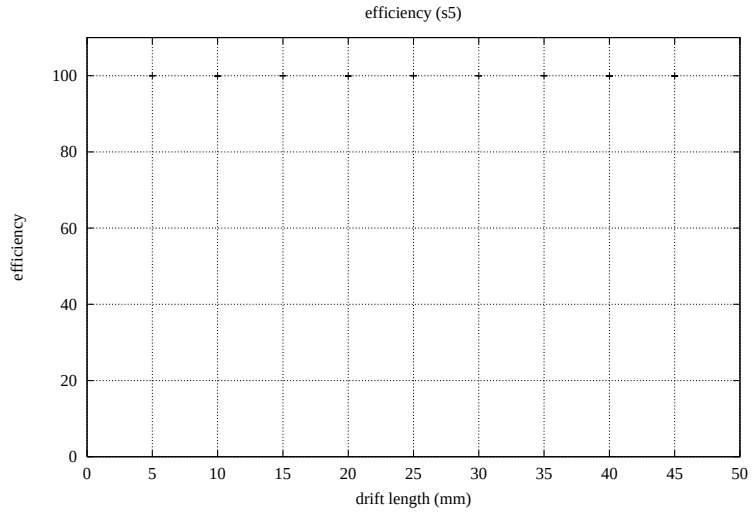

Figure 3.17: efficiency as a function of the drift distance for s5

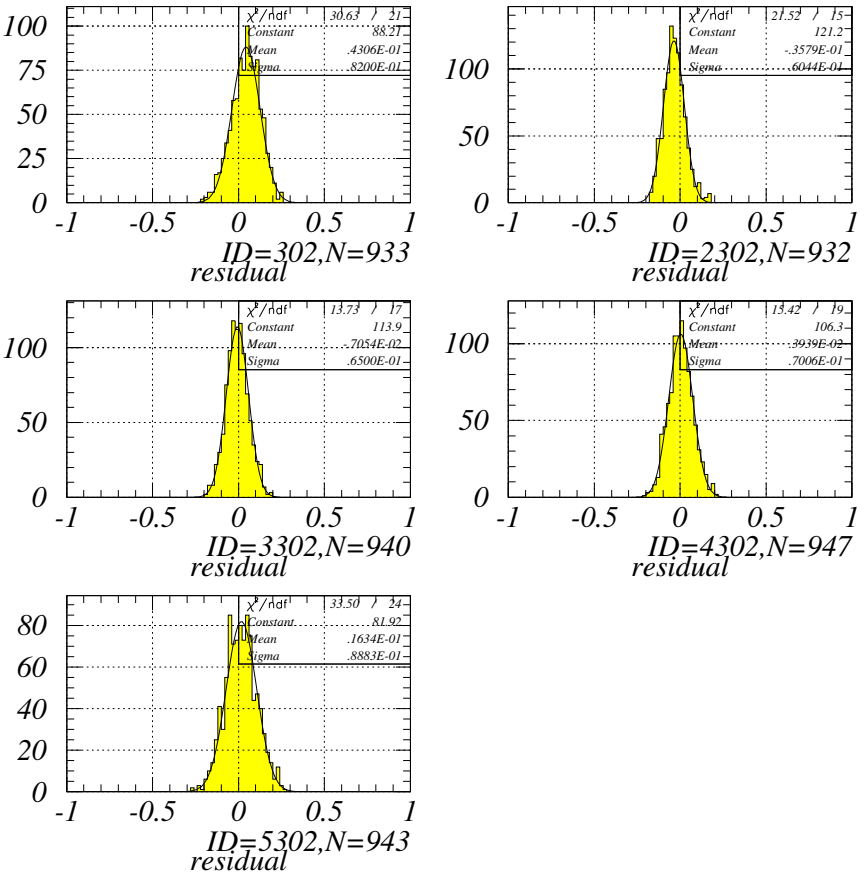

Figure 3.18: residual distributions for tracks with a drift distance of 2.5cm

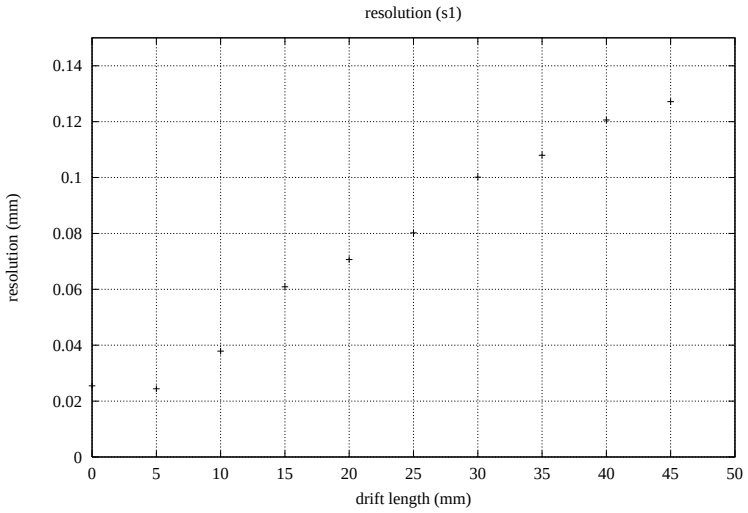

Figure 3.19: spatial resolution as a function of the drift distance for s1

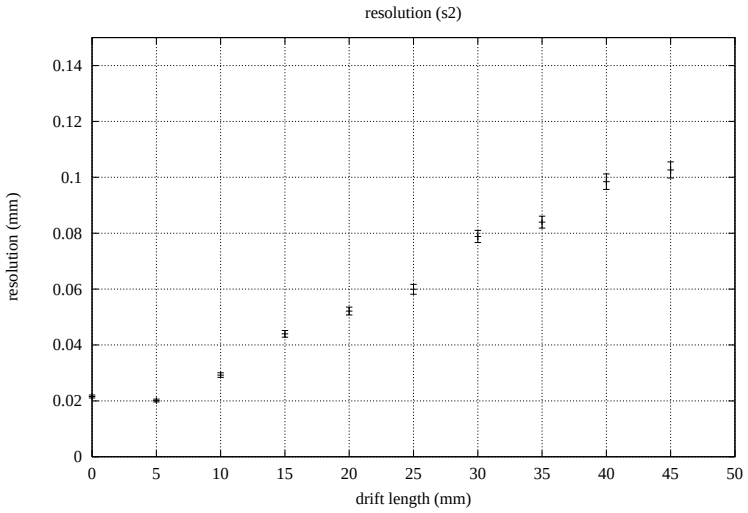

Figure 3.20: spatial resolution as a function of the drift distance for s2

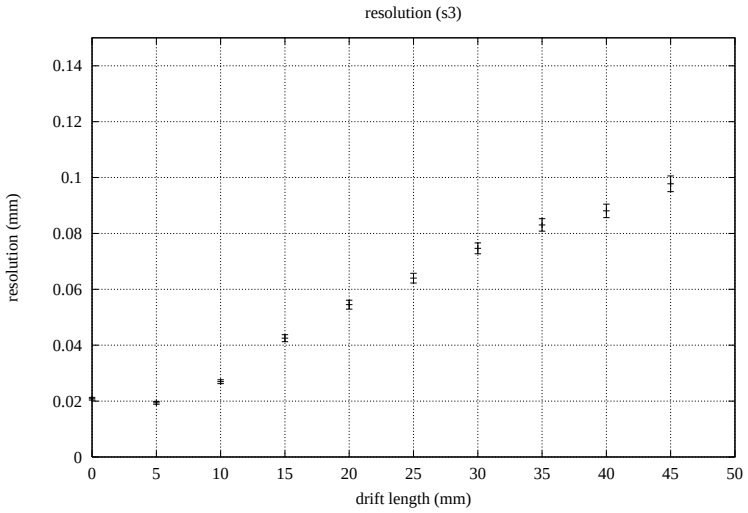

Figure 3.21: spatial resolution as a function of the drift distance for s3

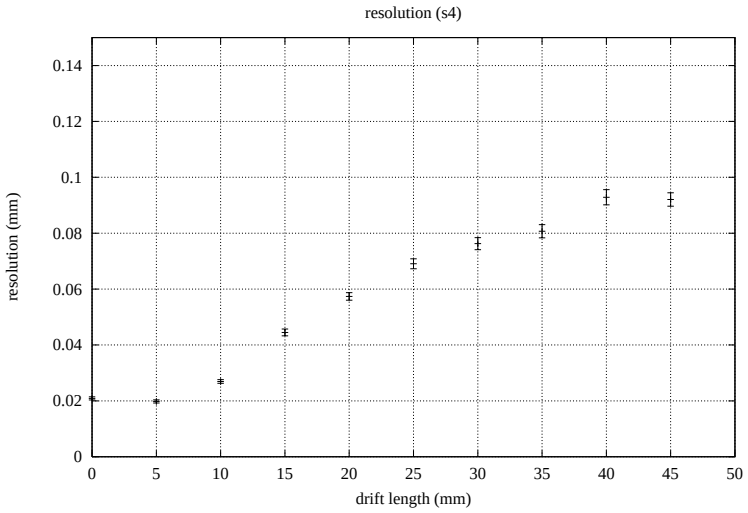

Figure 3.22: spatial resolution as a function of the drift distance for s4

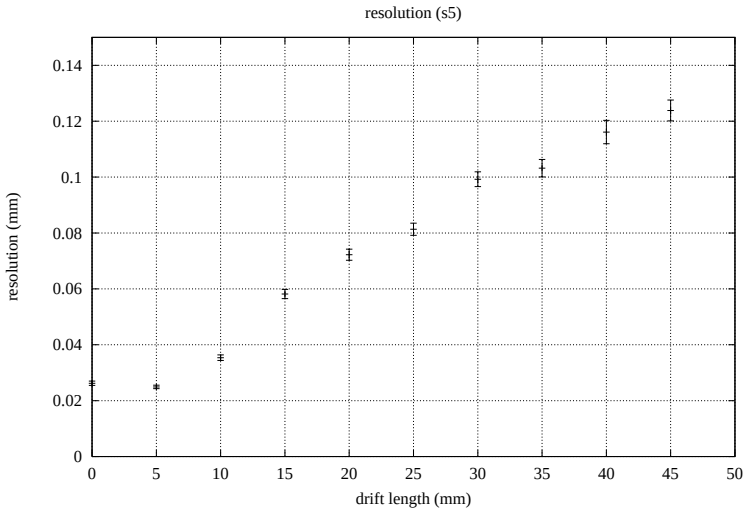

Figure 3.23: spatial resolution as a function of the drift distance for s5

height becomes smaller towards the edge of the drift region. It influences the spatial resolution.

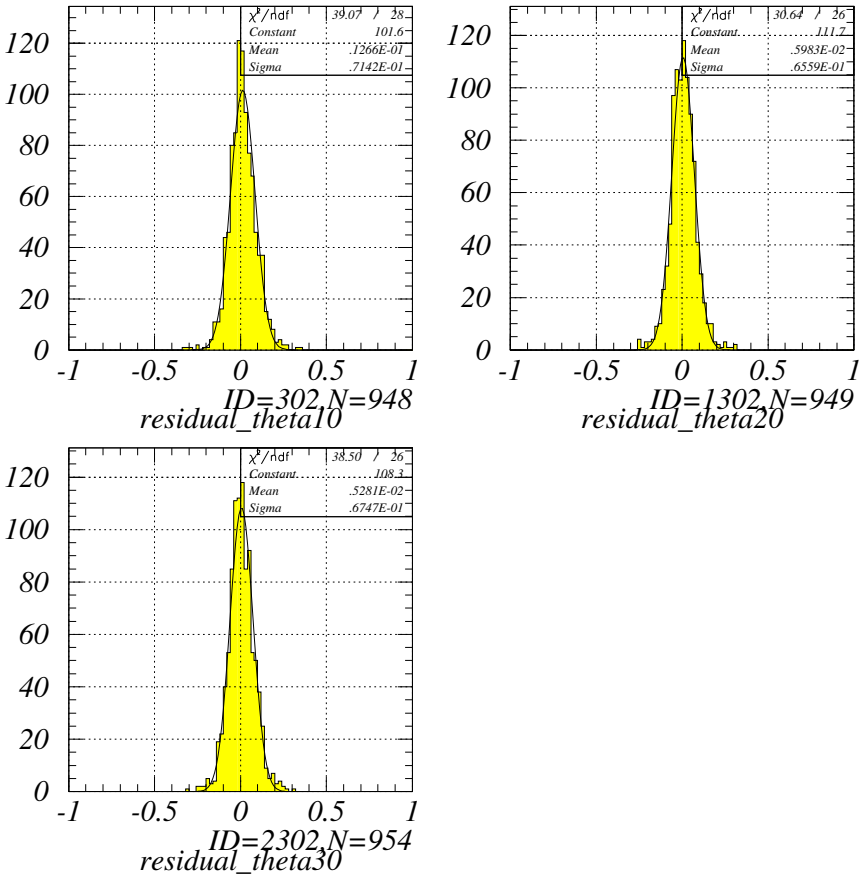

Figure 3.24: residual distributions for $\theta = 10°, 20°$, and $30°$ for the central sense wire (s3)

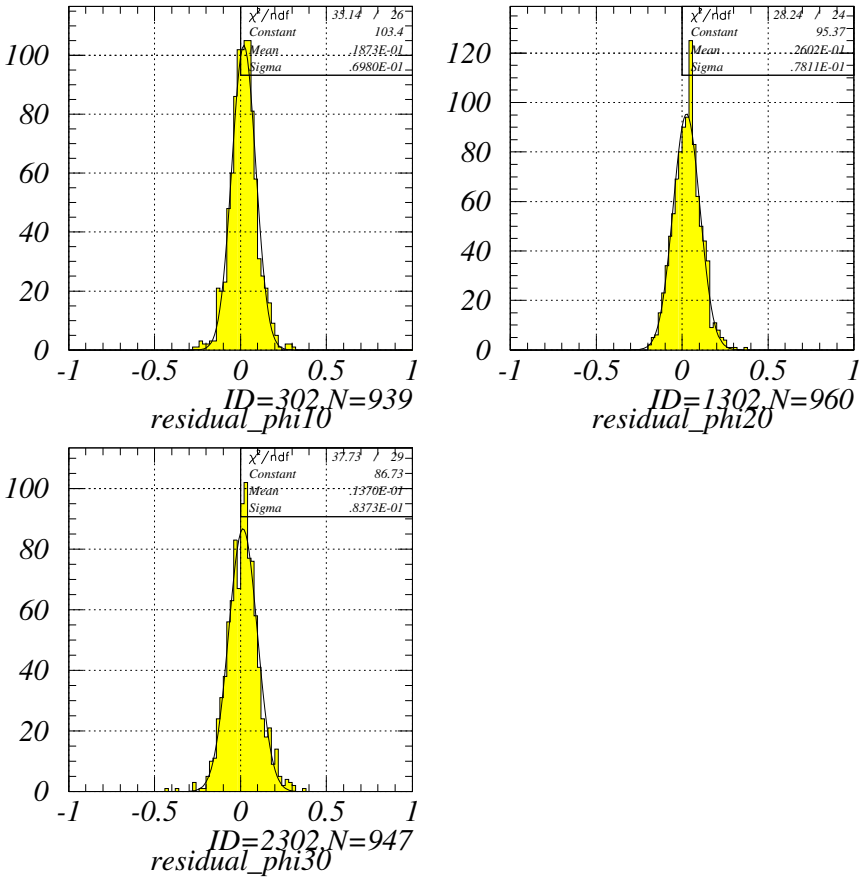

Figure 3.25: residual distributions for $\phi = 10°, 20°$, and $30°$ for the central sense wire (s3)

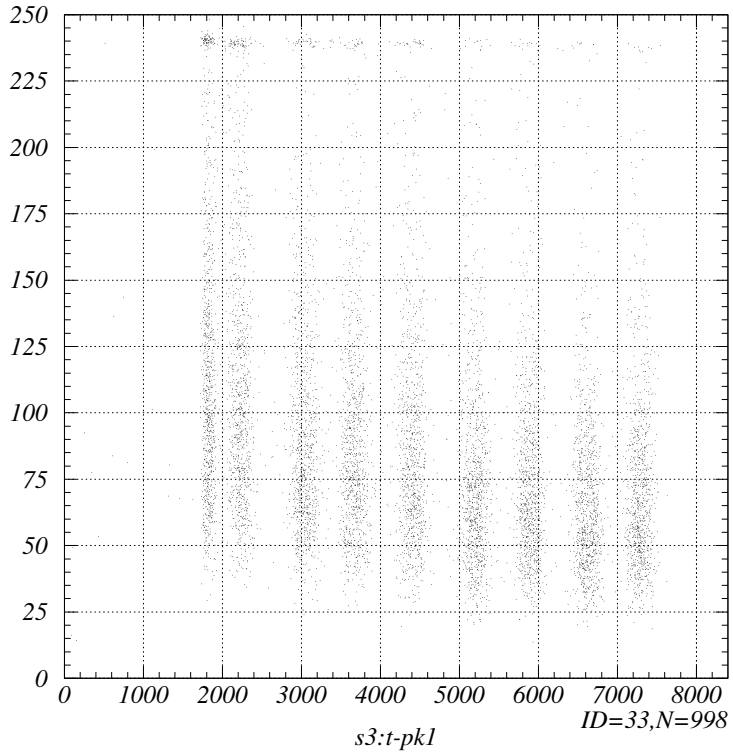

Figure 3.26: peak pulse height as a function of the drift time for the central sense wire (s3)

3.5 Two-track separation

3.5.1 Two-track separation probability

The separation efficiency of hits for two-track experiment is shown in figure 3.27 for the central sense wire (s3). In this analysis, we did track fitting with the signals on the four sense wires excluding the one to study and selected events with two tracks. We then required that there was an actual signal in the 5σ window about the first track, where *first* means closer to the sense wire. We then tested whether there was a real signal in the 5σ window about the second track. If there was a real signal, it was an efficient event. In figure 3.27, the horizontal axis is the distance between the first and the second tracks (mm). In the case of the distance being more than 6mm, the two-hit separation efficiency was almost 100%. When the distance was less than 5mm, the two-track separation capability became worse. This is at last partly due to the gas gain saturation problem.

The residual distributions for the first and the second tracks are shown in figure 3.28. The upper figure shows the residual distributions for the first tracks and the lower figure shows second tracks. The resolution for the second tracks was worse than the first tracks due mostly to their smaller pulse height.

And we analyzed the two-track experiment data by different means. First, we calculated the track distance in cell2. And then we calculated whether the track distance in cell1 was the same with the track distance in cell2. This result is shown in figure 3.29. In the case of the distance being more than 6mm, the two-hit separation efficiency was almost 100%. But, the distance was less than 5mm, the two-track separation capability became worse.

3.5.2 Effect of the gas gain saturation problem

Typical pulse shapes for inefficient events are shown in figures 3.30 and 3.31 for the central sense wire (s3). In figure 3.30, no signal on the sense wire #3 for the second track can be seen and in figure 3.31, the second pulse may be a real signal for the second track or *pulse2* for the first track. We consider that two-track separation capability can be heavily dependent on the gas gain saturation problem.

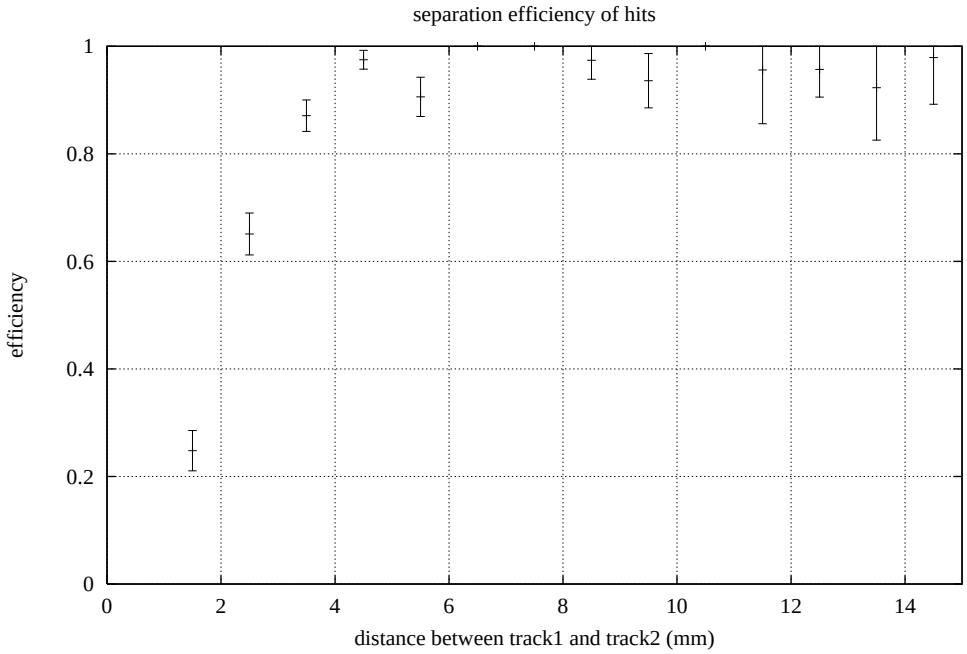

Figure 3.27: two-hit separation efficiency as a function of the drift distance for the central sense wire (s3)

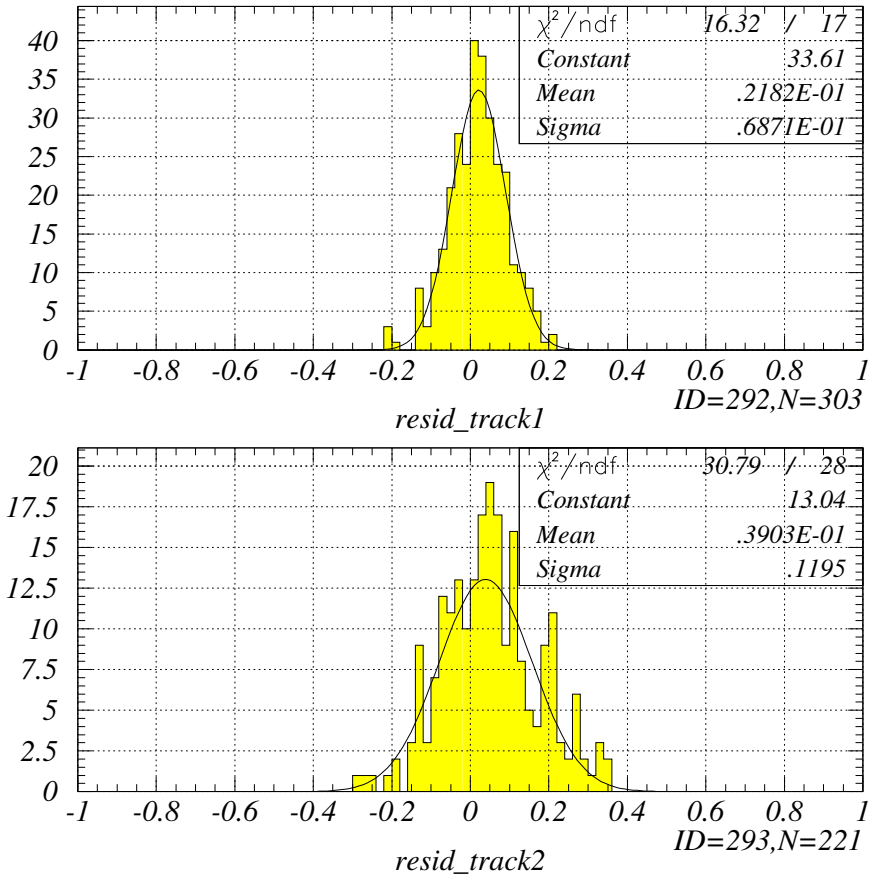

Figure 3.28: residual distributions first (upper) and second (lower) tracks for the central sense wire (s3)

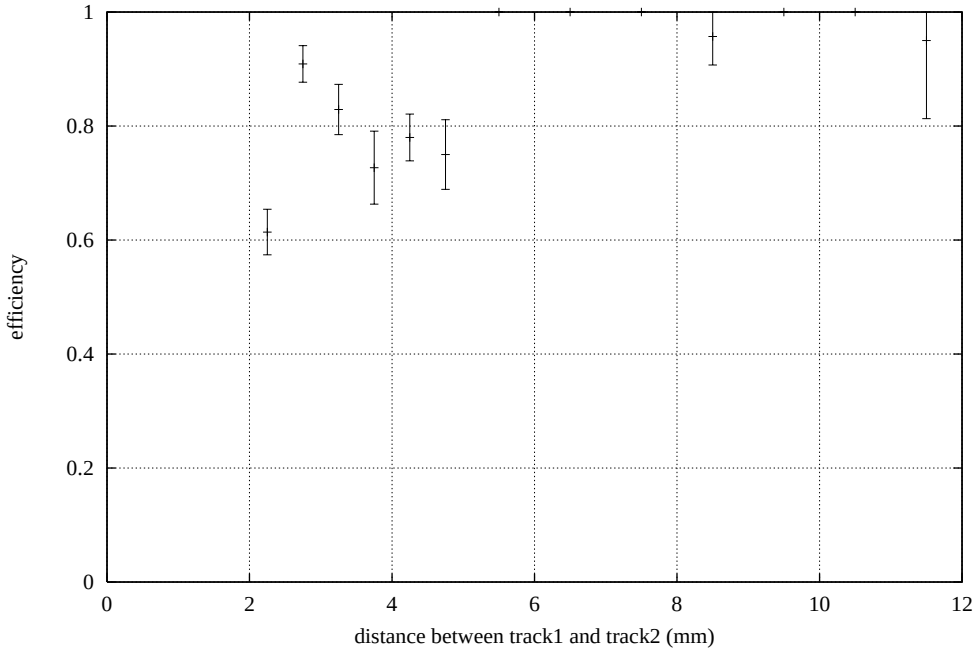

Figure 3.29: two-track separation efficiency in cell1 as a function of the drift distance for the central sense wire (s3)

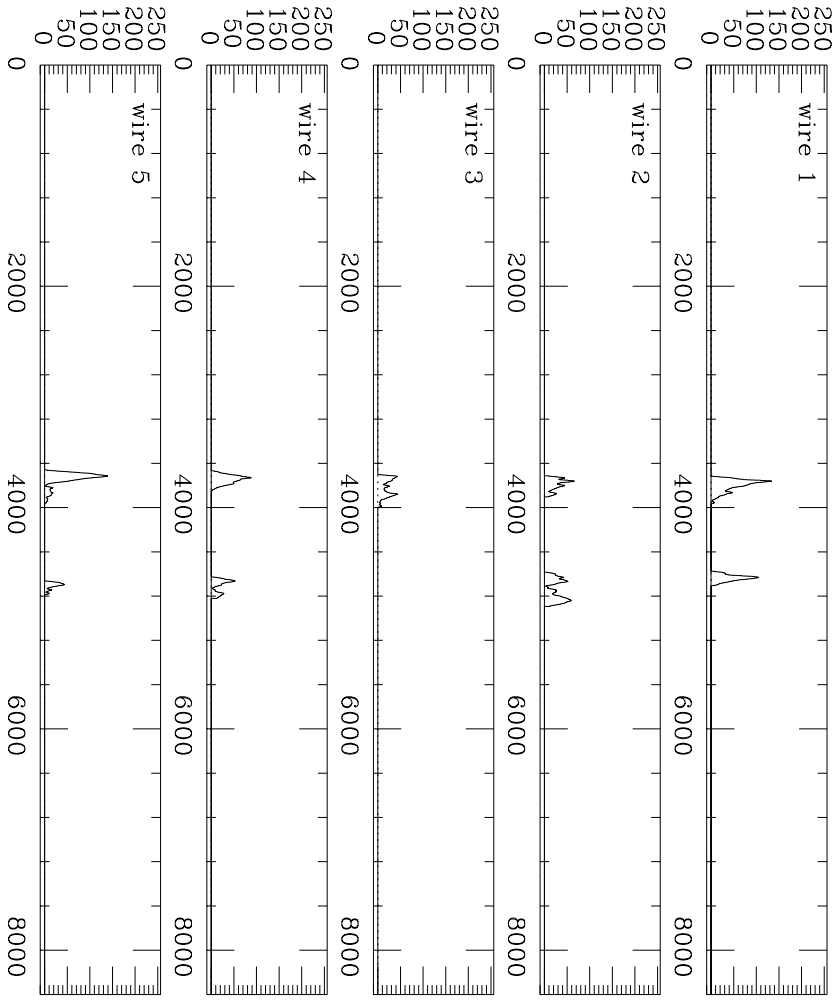

Figure 3.30: a typical inefficient event

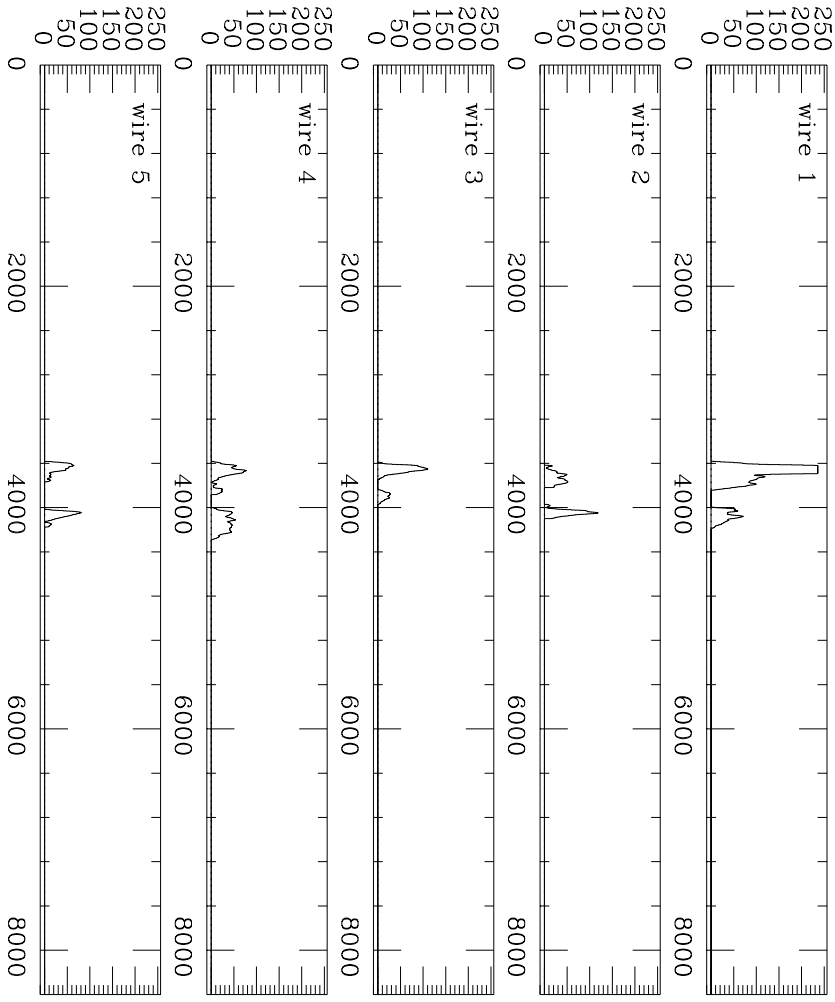

Figure 3.31: another example of inefficient events

Chapter 4

Conclusion

We have fabricated a small test chamber with the same jet cell structure as with our previous 4.6m-long test chamber, in order to carry out beam tests on basic chamber performance. The small test chamber was filled with a CO_2-isoC_4H_{10}(90:10) gas mixture and was exposed to test beams at KEK-Tanashi.

We used an extracted electron beam to study single track performance and confirmed that the test chamber satisfies the required spatial resolution of 100μm per wire over the full drift space, regardless of the incident angles θ and ϕ. In the course of this single track study, we found that more than 50% of the times, a main chamber signal pulse was followed by a smaller pulse, which is a potential problem for two-track separation. We have investigated this phenomenon and found it likely to be connected with a gas gain saturation effect.

In order to study two-track separation capability, we used a photon beam converted to e^+e^- pairs with an Al converter. We found that two tracks with a track distance greater than 5mm is identified without ambiguity. For two tracks with a track distance less than 5mm, however, we observed a siginificant efficiency drop. This efficiency drop might be coming from the dead time due to the gas gain saturation problem. This possibility is best discriminated by studying the dependence on the two-track distance in the wire direction. The data for this study are unfortunatelly not at hand, since our setup only allowed two-track separation in the drift direction: two tracks were almost always on top of each other when projected to the wires because the direction of the magnetic field to separate the e^+e^- pairs was parallel to

the wires. We are planning to make another beam test to study this effect next summer.

Chapter 5

Acknowledgment

I thank assistant professor O. Nitoh and Professor K. Takahashi for essential support. I acknowledge all the members of the chair of high energy physics at Tokyo University of Agriculture and Technology.

I would like to thank all the members of the JLC-CDC group, especially K. Fujii, Y. Kato, N. Khalatyan, Y. Kurihara, T. Matsui, H. Okuno, T. Watanabe, T. Yoshida, for help in the construction of the experimental set up, carrying out measurements and the analysis.

Lastly, I thank A. Yamaguchi for his help and discussion.

References

1. JLC group, KEK Report 92-16, December, 1992.

2. Y. Kurihara, A. Yamaguchi, S. Sudo, T. Abe, K. Fujii, N. Ishihara, N. Khalatyan, T. Matsui, O. Nitoh, T. Ohama, H. Okuno, A. Sugiyama, K. Takahashi, T. Watanabe, T. Yoshida, Cosmic Ray Tests of a 4.6m-long Test Drift Chamber for JLC, December, 1998.

3. N. Khalatyan, K. Fujii, H. Okuno, T. Abe, K. Hoshina, Y. Kato, Y. Kurihara, H. Kuroiwa, T. Matsui, O. Nitoh, A. Sugiyama, K. Takahashi, T. Watanabe, T. Yoshida, KEK Preprint 98-187 "Designing of Stereo-Wire Geometry for a Long Cylindrical Drift Chamber with Small Jet Cells", November, 1998.

4. A. Yamaguchi, Master's Thesis "Performance test of a prototype large jet chamber", 1998., in Japanese.

5. S. Sudo, Master's Thesis "Research and development of a large drift chamber with small jet cells", 1997., in Japanese.

6. Veen Hove, A Drift Chamber simulation program GARFIELD, 1994.